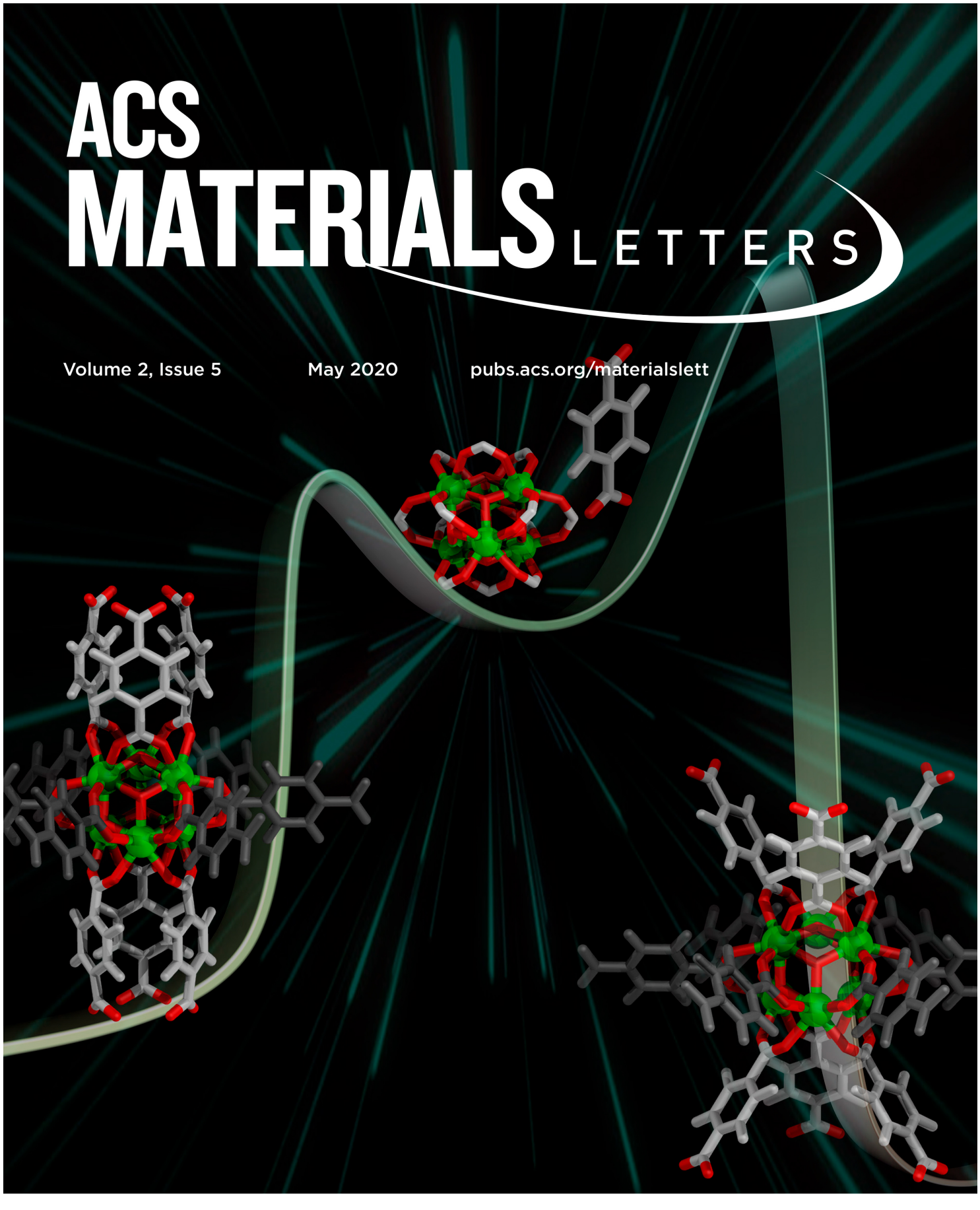

ACS Publications
Most Trusted. Most Cited. Most Read.

www.acs.org

ACS MATERIALS LETTERS

www.acsmaterialsletters.org

LETTER

Time-Resolved *in Situ* Polymorphic Transformation from One 12-Connected Zr-MOF to Another

Seung-Joon Lee, Jenna L. Mancuso, Khoa N. Le, Christos D. Malliakas, Youn-Sang Bae, Christopher H. Hendon,* Timur Islamoglu,* and Omar K. Farha*

Cite This: *ACS Materials Lett.* 2020, 2, 499−504

Read Online

ACCESS | Metrics & More | Article Recommendations | Supporting Information

ABSTRACT: Understanding polymorphism in metal−organic frameworks (MOFs) provides opportunities to unravel the process of MOF crystallization, and it enables the elucidation of structure−property relationships of compositionally identical crystals. Here, we present the modulator- and temperature-mediated polymorphic transformation of the kinetic product from Zr_6-based MOF synthesis, EHU-30, to the thermodynamic product, UiO-66. The partial dissolution−recrystallization process was demonstrated by a combination of *in situ* powder X-ray diffraction (PXRD) and *in situ* ^{1}H NMR spectroscopy where EHU-30 was heated in the presence of a monotopic acid modulator, acetic acid. Density functional theory (DFT) calculations show that the EHU-30 polymorph is less stable because the bent linkers have higher Gibbs free energy compared to linear linkers in the thermodynamic product, UiO-66.

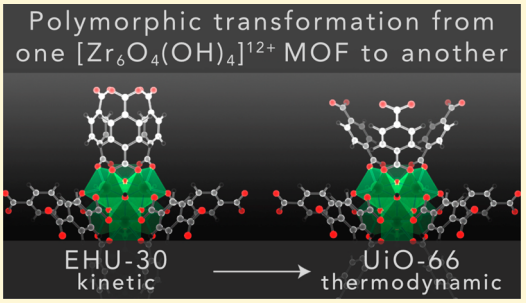

Metal−organic frameworks (MOFs), which self-assemble from organic linkers and metal clusters (or metal ions), are an exciting class of materials with unparalleled structural versatility. Researchers may tune these frameworks down to the atomic level, enabling systematic modulation and investigation that are impossible with many other solid-state materials.[1−6] Like zeolites, these high-symmetry networks exhibit complex topologies; however, MOFs display a range of other dynamic properties, such as breathing and negative gas adsorption.[7−15] Although the number of reported MOFs is steadily increasing, with over 90 000 MOF structures in Cambridge Structural Database,[16] the effort towards designing new MOFs with desired topologies focused on designing new linkers and the exploration of polymorphism in MOFs are rare.[17−28] While the theoretical construct for examining polymorphism exists, the discovery and interconversion between MOF polymorphs has been largely neglected due to interest in the intuitive thermodynamic assembly process.[29] Correspondingly, studies that monitor any aspect of the MOF assembly process *in situ* are rare.

In general, two types of polymorphic transformations have been widely recognized: (i) single-crystal-to-single-crystal transformation where the crystal integrity and the long-range structural order are maintained through the transformation process and (ii) dissolution−recrystallization transformation where the components of the crystals reassemble to form a different phase crystal.[30] Metastable kinetic products have been studied to convert into the stable thermodynamic form by applying the appropriate stimuli such as temperature, pressure, light, solvation, and guest molecule removal or exchange.[31−36] For example, the 8-connected Zr_6O_8 node with tetratopic linkers has been utilized to form different polymorphs by controlling the dihedral angle between the carboxylate bound phenyl and central pyrene, porphyrin, or benzene plane, and conversion of the metastable products to the more stable products was possible by altering the reaction conditions.[21,23,37−40] Similarly, conformational differences of ditopic linkers in the Zr-based MOFs have resulted in MOFs with different topologies.[41] These examples highlight that chemical space can be largely expanded if we consider that multitopic linkers are flexible species, rather than rigid pillars, and, in turn, should provide access to a diverse family of compositionally similar scaffolds.

Received: January 15, 2020
Accepted: April 6, 2020

https://dx.doi.org/10.1021/acsmaterialslett.0c00012
ACS Materials Lett. 2020, 2, 499−504

UiO-66, first reported in 2008,[42] is one of the most studied MOFs due to its ease of synthesis, exceptional stability, and its ability to be both pre- and postsynthetically functionalized.[43−46] While there are many reports of defect engineering in UiO-66, resulting in different topologies with different nominal stoichiometries,[47−49] there is only one reported polymorph of UiO-66, EHU-30.[50] Similar to UiO-66, EHU-30 has 12-connected Zr_6 nodes but rather crystallizes in a *hex* topology as opposed to a *fcu* topology. The structural dissimilarity arises from three distorted linkers per formula unit, shown schematically in Figure 1.

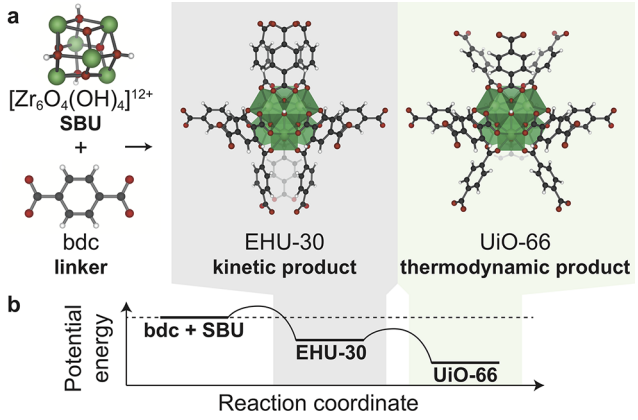

Figure 1. Schematic reaction energy profile and structure of kinetic product EHU-30 and thermodynamic product UiO-66 (C, black; H, pink; O, red; Zr, green).

Herein, we monitor *in situ* powder X-ray diffraction (PXRD) and *in situ* ^{1}H NMR spectroscopy to determine the structural conversion process of the modulator- and temperature-mediated polymorphic transformation from a kinetic product, EHU-30, to the thermodynamic product, UiO-66′ (where UiO-66′ is transformed EHU-30) (Figure 1). Scanning electron microscopy (SEM), thermogravimetric analysis (TGA), and gas adsorption isotherms complement the *in situ* measurements to reveal the necessity of both heat and acetic acid to convert EHU-30 to UiO-66′. Furthermore, density functional theory (DFT) is applied to identify the driving force of this transformation by comparing the linkers in UiO-66′ and the distorted linkers of EHU-30.

EHU-30 was synthesized based on the original reported scheme (see the Supporting Information for details).[50] Unlike the synthetic conditions for UiO-66 formation where concentration of the reaction solution is kept low,[51,52] EHU-30 was synthesized from a concentrated solution of methacrylic acid modulator; kinetic access to the first known metastable polymorph of UiO-66 was gained through an excess of modulator, which encourages prenucleation of the zirconia clusters.[50] The methacrylate node modulators template the less-stable polymorph connectivity and are replaced by benzene-1,4-dicarboxylic acid (BDC) over time.

Conversion to UiO-66′ was accomplished by heating a solution of EHU-30 and acetic acid in *N*,*N*-dimethylformamide (DMF). Comparing the PXRD patterns of samples transformed at different temperatures and volumetric ratios of DMF/acetic acid revealed both a temperature- and concentration-dependent path. Firstly, EHU-30 was suspended in DMF:acetic acid (DMF:acetic acid = 2:1, 3:1, or 5:1 v:v) and heated in the oven (80, 100, or 120 °C) for 20 h. Under all conditions, the transformation of EHU-30 to the thermodynamic product UiO-66′ was observed. PXRD patterns of each product suggest that higher temperatures and lower reaction concentrations favor UiO-66′ formation (Figure S1-3), consistent with the typical UiO-66 synthetic conditions.[38] Complete conversion of EHU-30 to UiO-66′ was achieved at 100 °C in DMF:acetic acid = 5:1 v:v (Figure 2).

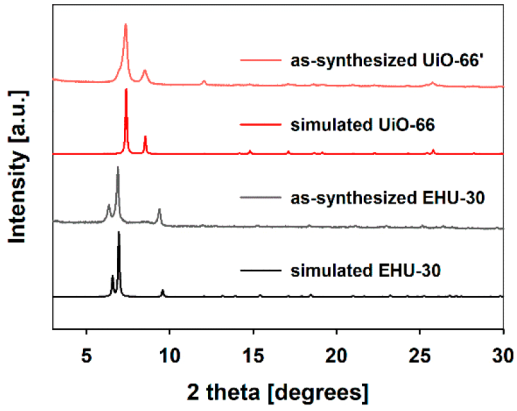

Figure 2. PXRD patterns (measured with Cu-radiation) of as-synthesized EHU-30 and UiO-66′ in mixed DMF/acetic acid solution (5:1 v:v, 100 °C, 20 h in oven) compared with simulated EHU-30 and UiO-66.

Unincorporated starting materials were removed by soaking the as-synthesized EHU-30 material in new batches of DMF for 3 days, until no further methacrylic acid or BDC was detected in the supernatant fluid by ^{1}H NMR (Figure S4a). The composition of each species was analyzed by ^{1}H NMR spectra of the digested parent EHU-30 and UiO-66′ in 1 M NaOD solution. The EHU-30 spectrum showed that approximately 17% of coordinated species were the methacrylic acid modulator rather than the BDC linker (Figure S5a). No methacrylate peaks were observed in the ^{1}H NMR of digested UiO-66′, indicating complete exchange of methacrylate for acetate during the transformation (Figure S5b). Acetate peaks, however, were observed. In either case, the presence of a modulator indicates missing linker type defects in both structures.

Analysis of ground state materials provides ample structural information; however, we sought to explore the relationship between polymorphs by examining intermediate species as well. PXRD experiments were therefore performed *in situ*. The reaction conditions from the oven were mimicked in a sealed capillary, and time-resolved *in situ* PXRD patterns were collected to follow the reaction; measurements were taken every 5 min for 12 h. The PXRD data showed the gradual disappearance of EHU-30 peaks (2θ = 5.4°, 6.9°, and 9.4°), with a concomitant increase in UiO-66′ peaks (2θ = 7.4° and 8.5°). Upon further analysis, the transformation process can be divided into three regions. The first region is the induction period; in the first 2 h no noticeable changes occur in the PXRD patterns. Both UiO-66 and EHU-30 feature strong bonds between Zr(IV) ions in the cluster and the carboxylate motif of BDC. An activation barrier must be overcome for the conversion process to occur (Figure S6). The transformation begins in the second region, from 2 to 6 h, during which three major EHU-30 peaks (2θ = 5.4°, 6.9°, and 9.4°) decrease, and two major peaks for the targeted, *fcu* topology of UiO-66

https://dx.doi.org/10.1021/acsmaterialslett.0c00012
ACS Materials Lett. 2020, 2, 499−504

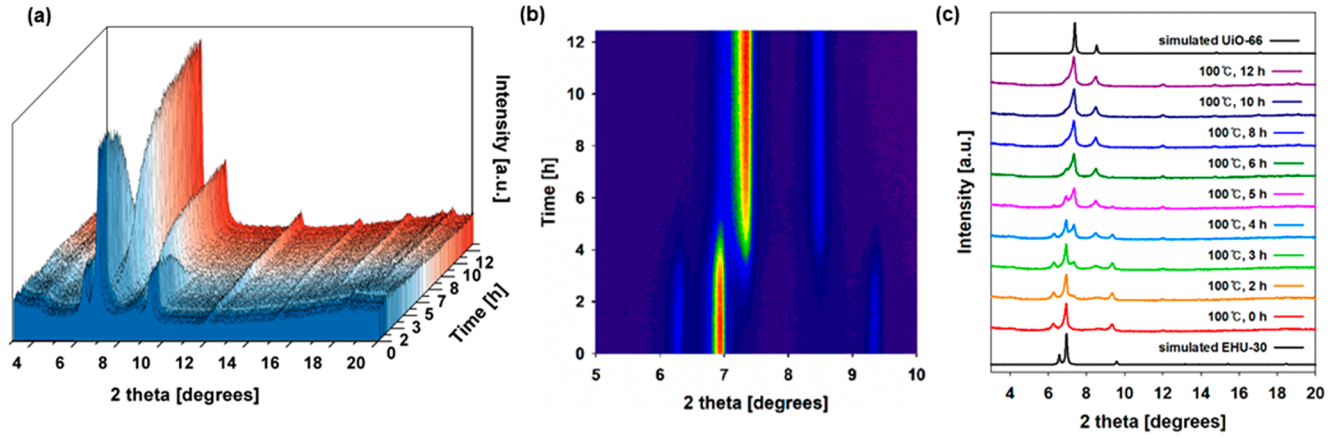

Figure 3. ***In situ*** **powder X-ray diffraction (measured with Cu-radiation) of EHU-30 at each reaction in 5:1 v:v DMF/acetic acid solutions at 100 °C over 12 h. (a) 3D graphics, (b) contour plot of the major peaks region 2θ = 5−10°, and (c) 2D graphics compared with simulated PXRD patterns of EHU-30 and UiO-66.**

emerge (2θ = 7.4° and 8.5°). In the third region, after 6 h, EHU-30 peaks in the PXRD pattern are nearly absent, while the intensity of UiO-66′ peaks continues to gradually increase. At the end of 12 h, the final PXRD pattern is in good agreement with simulated UiO-66, indicating the successful polymorphic transformation of EHU-30 to its thermodynamic minimum (Figure 3c). The scanning electron microscopy (SEM) images of EHU-30 and UiO-66′ showed a similar morphology with a similar particle size (Figure S8).

In order to differentiate between the dissolution−recrystallization process and a single crystal transformation, *in situ* ^{1}H NMR spectra were collected under the same reaction conditions. The initial ^{1}H NMR of EHU-30 (6 mg) suspended in DMF-d_7 (0.5 mL) did not show signals from BDC or methacrylic acid, supporting the complete removal of unreacted species from our modified washing procedure. A small amount (2 μL) of *N*-methyl-2-pyrrolidone (NMP) was added as an internal standard along with acetic acid-d_4 (0.1 mL). The reaction was allowed to proceed at 100 °C, and *in situ* ^{1}H NMR spectra were collected every 10 min for 12 h (Figure 4b). *Ex situ* ^{1}H NMR spectra were then collected until the system equilibrated, every 3 h up to 36 h (Figure 4c). Both BDC and methacrylic acid were observed in the first spectrum after acetic acid-d_4 addition (Figure S4b), which can be attributed to the displacement of dangling species on the crystal surface. Importantly, this also shows that acetic acid is involved in the decoordination of both BDC and methacrylate from the node. The relative concentrations of methacrylic acid and BDC (Figure 4c) showed a steep initial increase of methacrylic acid that reached equilibrium in ∼3 h. The facile removal of coordinated methacrylates indicates that they are replaced by acetic acid, and the plateau in final concentration shows that dissolved methacrylic acid neither participates in building the UiO-66′ phase nor is included in the thermodynamic product; this is supported by the absence of methacrylic acid peaks in the ^{1}H NMR spectra of digested UiO-66′ product after the reaction.

The concentration of dissolved BDC, however, initially increased in concentration, for ∼6 h, and then decreased in concentration as the reaction proceeded. The correlation between methacrylic acid and BDC signals indicates dissolution of linkers in EHU-30, followed by consumption of the free BDC linkers in solution and formation of UiO-66′, confirming that dissolution−recrystallization is an active component of the transformation. Coupled with the PXRD and incomplete dissolution of EHU-30, this result indicates a partial dissolution and recrystallization. The rate of methacrylate release is expected to be faster than BDC^{2-} because of the different energetic contribution of entropy when removing a monotopic or ditopic ligand. Notably, the BDC concentration in the equilibrated system is higher after the transformation is complete. The UiO-66′ phase, which incorporates acetic acid rather than methacrylic acid, is therefore more defective than the parent EHU-30 phase. Polymorphic transformations may provide a strategy to increase the concentration of missing linker defects, i.e., coordinatively unsaturated metal sites.

Importantly, both samples demonstrated permanent porosity; thus, the structural integrity of the crystal was maintained. N_2 physisorption isotherms were collected at 77 K (Figure S7). EHU-30 and UiO-66′ both exhibited steep initial uptake at low pressures, which indicates microporosity, consistent with the expected topology. Surface areas were calculated with the BET equation; EHU-30 and UiO-66′ were found to have apparent BET surface areas of 920 and 1070 m^2/g, respectively. Despite a higher geometric surface area that was estimated for EHU-30,[50] the observed higher surface area in UiO-66′ can be attributed to the defects present in the structure. Notably, we did not observe complete dissolution of EHU-30; complete disassembly of the parent framework may not be necessary to assemble UiO-66′. Both EHU-30 and UiO-66′ have six, coplanar linkers oriented in the same hexagonal net. The polymorphs differ in both the conformation and connectivity of the other six linkers. In UiO-66, they are connected to six different nodes such that all 12 linkers are equivalent at a pristine node. In the case of EHU-30, however, the other six linkers are split between only two nodes resulting in a significant amount of strain.

To assess the relative conformational stability of linkers in each MOF, density functional theory (DFT) was employed to determine the energetic penalty for linker distortion in EHU-30. The difference in energy between the bent and linear conformations was found through linker models extracted from the bulk optimized structures of EHU-30 and UiO-66′ in order to isolate the effect of linker distortion (Figure 5). The difference in Gibbs free energy, a measure of strain, was found to be ∼3.0 kcal/mol. In conjunction with the incomplete dissolution of EHU-30 observed *in situ*, we hypothesized that

https://dx.doi.org/10.1021/acsmaterialslett.0c00012
ACS Materials Lett. 2020, 2, 499−504

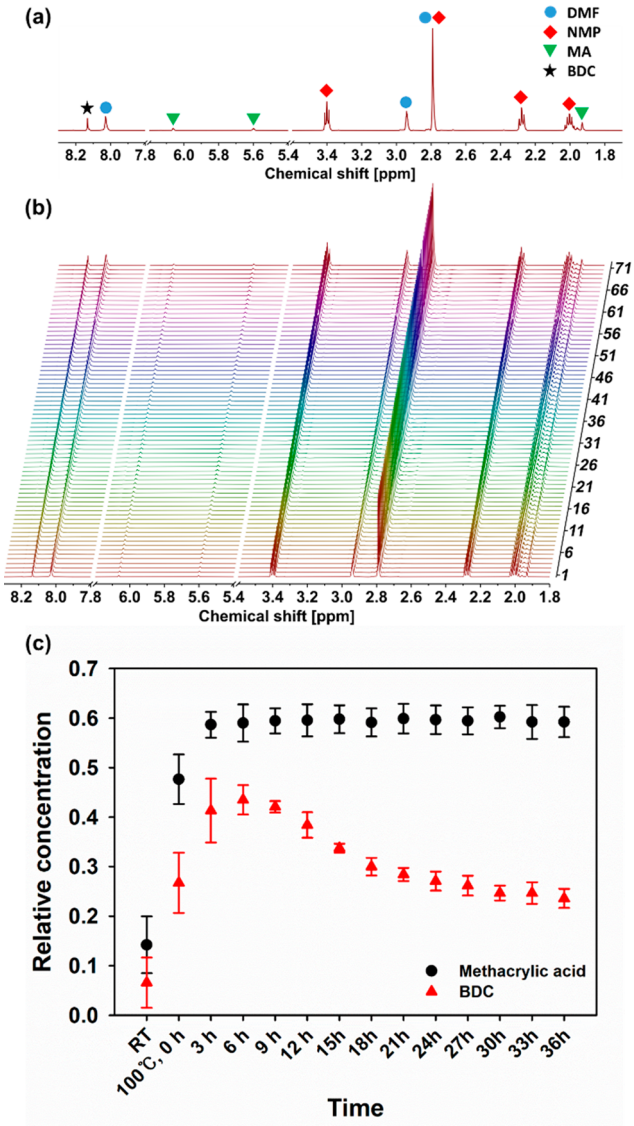

Figure 4. (a) Final *in situ* ^{1}H NMR measurement of EHU-30 collected after 12 h (DMF, *N*,*N*-dimethylformamide; NMP, *N*-methyl-2-pyrrolidone; MA, methacrylic acid; BDC, 1,4-benzenedicarboxylic acid). (b) *In situ* ^{1}H NMR measurements of EHU-30 every 10 min at 100 °C for 12 h. (c) Relative concentration of dissolved methacrylic acid and BDC via combined *in situ* (RT, 12 h) and *ex situ* (12−36 h) ^{1}H NMR results of EHU-30. Error bars represent standard deviation in three different batches of measurements.

the population of disconnected linkers observed by NMR was dominated by the formerly bent linkers, which disconnect from the node and reorganize to form the more stable UiO-66 *fcu* topology. The computed densities of states are further presented for each polymorph, to demonstrate that both polymorphs are expected to have similar photophysical properties, with their optical gap governed by a ligand-to-ligand transitions occurring in the UV.

As mentioned earlier, in EHU-30 about 17% of BDC^{2-} positions are occupied by methacrylate, which is completely leached into the solution during the phase transformation. With knowledge of the final methacrylic acid concentration in the solution, we estimated the amount of BDC in the solution to be ∼12% after 6 h (Figure 4c). However, this does not necessarily mean that only 12% of the linkers are involved in

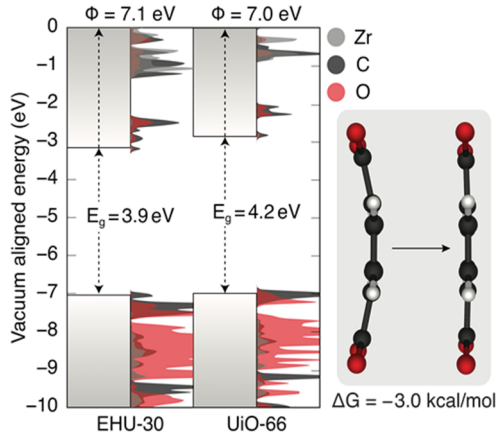

Figure 5. Band edge diagram and theoretical density of states for EHU-30 and UiO-66 demonstrating a subtle difference in frontier band characteristics. A depiction of the bent and linear linkers is additionally presented to illustrate the strain energy stored in the BDC units of EHU-30.

phase transformation, since this 12% only represents free BDC in solution. Mono-coordinated BDC linkers still will not show up in solution NMR. Additionally, the bond breaking/forming time scale can also be faster than the NMR spectra collection time. These results were in line with the *in situ* PXRD results, since it showed the coexistence of both phases.

In summary, we showed the modulator- and temperature-mediated polymorphic transformation of a kinetic MOF product, EHU-30, into its thermodynamic form, UiO-66. The rate of EHU-30 conversion showed a positive correlation with temperature and an inverse correlation with reaction concentration; the conversion conditions are closely related to the synthetic conditions of UiO-66. By monitoring reaction progress with *in situ* PXRD and ^{1}H NMR, and probing the energetic relationship between EHU-30 and UiO-66′ with DFT, it was found that EHU-30 undergoes a partial dissolution−recrystallization process driven by the rearrangement of linkers to release strain. Therefore, efforts to understand the relationship between kinetic and thermodynamic MOF products and characterizing the intermediate phases of transitions between them will inform the general design of synthetic parameters to target certain phases, which includes the formation of intrinsic defects as well as connectivity.

■ ASSOCIATED CONTENT

Supporting Information

The Supporting Information is available free of charge at https://pubs.acs.org/doi/10.1021/acsmaterialslett.0c00012.

Detailed description of synthesis, characterization, and modeling; and additional experimental results of PXRD, ^{1}H NMR, TGA, N_2 isotherms, and SEM images (PDF)

■ AUTHOR INFORMATION

Corresponding Authors

Christopher H. Hendon − *Department of Chemistry and Biochemistry, University of Oregon, Eugene, Oregon 97403, United States;* orcid.org/0000-0002-7132-768X; Email: chendon@uoregon.edu

Timur Islamoglu − *Department of Chemistry and International Institute of Nanotechnology, Northwestern University, Evanston,*

https://dx.doi.org/10.1021/acsmaterialslett.0c00012
ACS Materials Lett. 2020, 2, 499−504

Illinois 60208, United States; orcid.org/0000-0003-3688-9158; Email: timur.islamoglu@northwestern.edu

Omar K. Farha − *Department of Chemistry and International Institute of Nanotechnology, Northwestern University, Evanston, Illinois 60208, United States;* orcid.org/0000-0002-9904-9845; Email: o-farha@northwestern.edu

Authors

Seung-Joon Lee − *Department of Chemistry and International Institute of Nanotechnology, Northwestern University, Evanston, Illinois 60208, United States; Department of Chemical and Biomolecular Engineering, Yonsei University, Seoul 03722, Republic of Korea*

Jenna L. Mancuso − *Department of Chemistry and Biochemistry, University of Oregon, Eugene, Oregon 97403, United States*

Khoa N. Le − *Department of Chemistry and Biochemistry, University of Oregon, Eugene, Oregon 97403, United States*

Christos D. Malliakas − *Department of Chemistry and International Institute of Nanotechnology, Northwestern University, Evanston, Illinois 60208, United States;* orcid.org/0000-0003-4416-638X

Youn-Sang Bae − *Department of Chemical and Biomolecular Engineering, Yonsei University, Seoul 03722, Republic of Korea;* orcid.org/0000-0002-3447-4058

Complete contact information is available at: https://pubs.acs.org/10.1021/acsmaterialslett.0c00012

Notes

The authors declare no competing financial interest.

■ ACKNOWLEDGMENTS

O.K.F. gratefully acknowledges support from the Defense Threat Reduction Agency (HDTRA1-19-1-0007). This research was supported in part by Basic Science Research Program through the National Research Foundation of Korea (NRF) funded by the Ministry of Education (2018R1A6A3A01011909). This work was also supported in part by the Yonsei University Research Fund (Yonsei Frontier Lab, Young Researcher Supporting Program) of 2018. PXRD and NMR studies made use of the IMSERC at Northwestern University, which has received support from the Soft and Hybrid Nanotechnology Experimental (SHyNE) Resource (NSF ECCS-1542205), the State of Illinois, and the International Institute for Nanotechnology (IIN); SEM study made use of EPIC facility of Northwestern University's NU*ANCE* Center, which has received support from the SHyNE, the MRSEC program (NSF DMR-1720139) at the Materials Research Center, IIN, and the Keck Foundation. Computational works were performed using the High-Performance Computing cluster at the University of Oregon (Talapas), the Extreme Science and Engineering Discovery Environment (XSEDE) which is supported by National Science Foundation grant number ACI-1548562, and the Portland State University machine, Coeus, which is supported by the NSF (DMS1624776).

■ REFERENCES

(1) Bradshaw, D.; Claridge, J. B.; Cussen, E. J.; Prior, T. J.; Rosseinsky, M. J. Design, Chirality, and Flexibility in Nanoporous Molecule-Based Materials. *Acc. Chem. Res.* **2005**, *38*, 273−282.

(2) Perry, J. J., IV; Perman, J. A.; Zaworotko, M. J. Design and Synthesis of Metal-Organic Frameworks Using Metal-Organic Polyhedra as Supermolecular Building Blocks. *Chem. Soc. Rev.* **2009**, *38*, 1400−1417.

(3) Furukawa, H.; Cordova, K. E.; O'Keeffe, M.; Yaghi, O. M. The Chemistry and Applications of Metal-Organic Frameworks. *Science* **2013**, *341*, 1230444.

(4) Jiang, H. L.; Makal, T. A.; Zhou, H. C. Interpenetration Control in Metal-Organic Frameworks for Functional Applications. *Coord. Chem. Rev.* **2013**, *257*, 2232−2249.

(5) Furukawa, S.; Reboul, J.; Diring, S.; Sumida, K.; Kitagawa, S. Structuring of Metal-Organic Frameworks at the Mesoscopic/Macroscopic Scale. *Chem. Soc. Rev.* **2014**, *43*, 5700−5734.

(6) Islamoglu, T.; Goswami, S.; Li, Z.; Howarth, A. J.; Farha, O. K.; Hupp, J. T. Postsynthetic Tuning of Metal-Organic Frameworks for Targeted Applications. *Acc. Chem. Res.* **2017**, *50*, 805−813.

(7) Millange, F.; Medina, M. I.; Guillou, N.; Ferey, G.; Golden, K. M.; Walton, R. I. Time-Resolved in Situ Diffraction Study of the Solvothermal Crystallization of Some Prototypical Metal-Organic Frameworks. *Angew. Chem., Int. Ed.* **2010**, *49*, 763−766.

(8) Alhamami, M.; Doan, H.; Cheng, C. H. A Review on Breathing Behaviors of Metal-Organic-Frameworks (MOFs) for Gas Adsorption. *Materials* **2014**, *7*, 3198−3250.

(9) Murdock, C. R.; Hughes, B. C.; Lu, Z.; Jenkins, D. M. Approaches for Synthesizing Breathing MOFs by Exploiting Dimensional Rigidity. *Coord. Chem. Rev.* **2014**, *258*, 119−136.

(10) Schneemann, A.; Bon, V.; Schwedler, I.; Senkovska, I.; Kaskel, S.; Fischer, R. A. Flexible Metal-Organic Frameworks. *Chem. Soc. Rev.* **2014**, *43*, 6062−6096.

(11) Horike, S.; Shimomura, S.; Kitagawa, S. Soft Porous Crystals. *Nat. Chem.* **2009**, *1*, 695−704.

(12) Zhang, J.-P.; Zhou, H.-L.; Zhou, D.-D.; Liao, P.-Q.; Chen, X.-M. Controlling Flexibility of Metal−Organic Frameworks. *Natl. Sci. Rev.* **2018**, *5*, 907−919.

(13) Shivanna, M.; Yang, Q. Y.; Bajpai, A.; Patyk-Kazmierczak, E.; Zaworotko, M. J. A Dynamic and Multi-Responsive Porous Flexible Metal-Organic Material. *Nat. Commun.* **2018**, *9*, 3080.

(14) Zhang, Y.; Zhang, X.; Lyu, J.; Otake, K. I.; Wang, X.; Redfern, L. R.; Malliakas, C. D.; Li, Z.; Islamoglu, T.; Wang, B.; Farha, O. K. A Flexible Metal-Organic Framework with 4-Connected Zr6 Nodes. *J. Am. Chem. Soc.* **2018**, *140*, 11179−11183.

(15) Krause, S.; Bon, V.; Senkovska, I.; Stoeck, U.; Wallacher, D.; Tobbens, D. M.; Zander, S.; Pillai, R. S.; Maurin, G.; Coudert, F. X.; Kaskel, S. A Pressure-Amplifying Framework Material with Negative Gas Adsorption Transitions. *Nature* **2016**, *532*, 348−352.

(16) *Cambridge Crystallographic Data Centre (CCDC) The Cambridge Structural Database Hits One Million Structures*. https://www.chemistryworld.com/news/the-cambridge-structural-database-hits-one-million-structures/3010524.article#.XPjeOqBJlVg.twitter (June 6, 2019).

(17) Bueken, B.; Reinsch, H.; Heidenreich, N.; Vandekerkhove, A.; Vermoortele, F.; Kirschhock, C. E. A.; Stock, N.; De Vos, D.; Ameloot, R. An in Situ Investigation of the Water-Induced Phase Transformation of UTSA-74 to MOF-74(Zn). *CrystEngComm* **2017**, *19*, 4152−4156.

(18) Carson, F.; Su, J.; Platero-Prats, A. E.; Wan, W.; Yun, Y. F.; Samain, L.; Zou, X. D. Framework Isomerism in Vanadium Metal-Organic Frameworks: MIL-88B(V) and MIL-101(V). *Cryst. Growth Des.* **2013**, *13*, 5036−5044.

(19) Chaemchuen, S.; Zhou, K.; Yusubov, M. S.; Postnikov, P. S.; Klomkliang, N.; Verpoort, F. Solid-State Transformation in Porous Metal-Organic Frameworks Based on Polymorphic-Pillared Net Structure: Generation of Tubular Shaped MOFs. *Microporous Mesoporous Mater.* **2019**, *278*, 99−104.

(20) Frahm, D.; Hoffmann, F.; Froba, M. Two Metal-Organic Frameworks with a Tetratopic Linker: Solvent-Dependent Polymorphism and Postsynthetic Bromination. *Cryst. Growth Des.* **2014**, *14*, 1719−1725.

(21) Gong, X.; Noh, H.; Gianneschi, N. C.; Farha, O. K. Interrogating Kinetic Versus Thermodynamic Topologies of Metal-Organic Frameworks via Combined Transmission Electron Micros-

copy and X-Ray Diffraction Analysis. *J. Am. Chem. Soc.* **2019**, *141*, 6146−6151.
(22) Katsenis, A. D.; Puskaric, A.; Strukil, V.; Mottillo, C.; Julien, P. A.; Uzarevic, K.; Pham, M. H.; Do, T. O.; Kimber, S. A.; Lazic, P.; Magdysyuk, O.; Dinnebier, R. E.; Halasz, I.; Friscic, T. In Situ X-Ray Diffraction Monitoring of a Mechanochemical Reaction Reveals a Unique Topology Metal-Organic Framework. *Nat. Commun.* **2015**, *6*, 6662.
(23) Shaikh, S. M.; Usov, P. M.; Zhu, J.; Cai, M.; Alatis, J.; Morris, A. J. Synthesis and Defect Characterization of Phase-Pure Zr-MOFs Based on Meso-Tetracarboxyphenylporphyrin. *Inorg. Chem.* **2019**, *58*, 5145−5153.
(24) Wen, L.; Cheng, P.; Lin, W. Solvent-Induced Single-Crystal to Single-Crystal Transformation of a 2D Coordination Network to a 3D Metal-Organic Framework Greatly Enhances Porosity and Hydrogen Uptake. *Chem. Commun.* **2012**, *48*, 2846−2848.
(25) Jiang, H. L.; Tatsu, Y.; Lu, Z. H.; Xu, Q. Non-, Micro-, and Mesoporous Metal-Organic Framework Isomers: Reversible Transformation, Fluorescence Sensing, and Large Molecule Separation. *J. Am. Chem. Soc.* **2010**, *132*, 5586−5587.
(26) Lan, Y. Q.; Jiang, H. L.; Li, S. L.; Xu, Q. Solvent-Induced Controllable Synthesis, Single-Crystal to Single-Crystal Transformation and Encapsulation of Alq3 for Modulated Luminescence in (4,8)-Connected Metal-Organic Frameworks. *Inorg. Chem.* **2012**, *51*, 7484−7491.
(27) Akimbekov, Z.; Katsenis, A. D.; Nagabhushana, G. P.; Ayoub, G.; Arhangelskis, M.; Morris, A. J.; Friscic, T.; Navrotsky, A. Experimental and Theoretical Evaluation of the Stability of True MOF Polymorphs Explains Their Mechanochemical Interconversions. *J. Am. Chem. Soc.* **2017**, *139*, 7952−7957.
(28) Lyu, J.; Gong, X.; Lee, S. J.; Gnanasekaran, K.; Zhang, X.; Wasson, M. C.; Wang, X.; Bai, P.; Guo, X.; Gianneschi, N. C.; Farha, O. K. Phase Transitions in Metal-Organic Frameworks Directly Monitored through *In situ* Variable Temperature Liquid-Cell Transmission Electron Microscopy and in Situ X-Ray Diffraction. *J. Am. Chem. Soc.* **2020**, *142*, 4609−4615.
(29) Shen, P.; He, W. W.; Du, D. Y.; Jiang, H. L.; Li, S. L.; Lang, Z. L.; Su, Z. M.; Fu, Q.; Lan, Y. Q. Solid-State Structural Transformation Doubly Triggered by Reaction Temperature and Time in 3D Metal-Organic Frameworks: Great Enhancement of Stability and Gas Adsorption. *Chem. Sci.* **2014**, *5*, 1368−1374.
(30) Van Vleet, M. J.; Weng, T.; Li, X.; Schmidt, J. R. *In Situ*, Time-Resolved, and Mechanistic Studies of Metal-Organic Framework Nucleation and Growth. *Chem. Rev.* **2018**, *118*, 3681−3721.
(31) Zaczek, A. J.; Catalano, L.; Naumov, P.; Korter, T. M. Mapping the Polymorphic Transformation Gateway Vibration in Crystalline 1,2,4,5-Tetrabromobenzene. *Chem. Sci.* **2019**, *10*, 1332−1341.
(32) Wang, K.; Liu, J.; Yang, K.; Liu, B. B.; Zou, B. High-Pressure-Induced Polymorphic Transformation of Maleic Hydrazide. *J. Phys. Chem. C* **2014**, *118*, 8122−8127.
(33) Mir, M. H.; Koh, L. L.; Tan, G. K.; Vittal, J. J. Single-Crystal to Single-Crystal Photochemical Structural Transformations of Interpenetrated 3 D Coordination Polymers by [2+2] Cycloaddition Reactions. *Angew. Chem., Int. Ed.* **2010**, *49*, 390−393.
(34) Bobrovs, R.; Seton, L.; Actins, A. Solvent-Mediated Phase Transformation between Two Tegafur Polymorphs in Several Solvents. *CrystEngComm* **2014**, *16*, 10581−10591.
(35) Chen, X. D.; Zhao, X. H.; Chen, M.; Du, M. A 3D Copper(II) Coordination Framework Showing Different Kinetic and Thermodynamic Crystal Transformations through Removal of Guest Water Cubes. *Chem. - Eur. J.* **2009**, *15*, 12974−12977.
(36) Qin, T.; Gong, J.; Ma, J.; Wang, X.; Wang, Y.; Xu, Y.; Shen, X.; Zhu, D. A 3D MOF Showing Unprecedented Solvent-Induced Single-Crystal-to-Single-Crystal Transformation and Excellent CO_2 Adsorption Selectivity at Room Temperature. *Chem. Commun.* **2014**, *50*, 15886−15889.
(37) Karadeniz, B.; Zilic, D.; Huskic, I.; Germann, L. S.; Fidelli, A. M.; Muratovic, S.; Loncaric, I.; Etter, M.; Dinnebier, R. E.; Barisic, D.; Cindro, N.; Islamoglu, T.; Farha, O. K.; Friscic, T.; Uzarevic, K. Controlling the Polymorphism and Topology Transformation in Porphyrinic Zirconium Metal-Organic Frameworks via Mechanochemistry. *J. Am. Chem. Soc.* **2019**, *141*, 19214−19220.
(38) Bai, Y.; Dou, Y.; Xie, L. H.; Rutledge, W.; Li, J. R.; Zhou, H. C. Zr-Based Metal-Organic Frameworks: Design, Synthesis, Structure, and Applications. *Chem. Soc. Rev.* **2016**, *45*, 2327−2367.
(39) Lyu, J. F.; Zhang, X.; Otake, K.; Wang, X. J.; Li, P.; Li, Z. Y.; Chen, Z. J.; Zhang, Y. Y.; Wasson, M. C.; Yang, Y.; Bai, P.; Guo, X. H.; Islamoglu, T.; Farha, O. K. Topology and Porosity Control of Metal-Organic Frameworks through Linker Functionalization. *Chem. Sci.* **2019**, *10*, 1186−1192.
(40) Wasson, M. C.; Lyu, J. F.; Islamoglu, T.; Farha, O. K. Linker Competition within a Metal Organic Framework for Topological Insights. *Inorg. Chem.* **2019**, *58*, 1513−1517.
(41) Yuan, S.; Zou, L.; Li, H.; Chen, Y. P.; Qin, J.; Zhang, Q.; Lu, W.; Hall, M. B.; Zhou, H. C. Flexible Zirconium Metal-Organic Frameworks as Bioinspired Switchable Catalysts. *Angew. Chem., Int. Ed.* **2016**, *55*, 10776−10780.
(42) Cavka, J. H.; Jakobsen, S.; Olsbye, U.; Guillou, N.; Lamberti, C.; Bordiga, S.; Lillerud, K. P. A New Zirconium Inorganic Building Brick Forming Metal Organic Frameworks with Exceptional Stability. *J. Am. Chem. Soc.* **2008**, *130*, 13850−13851.
(43) Kandiah, M.; Nilsen, M. H.; Usseglio, S.; Jakobsen, S.; Olsbye, U.; Tilset, M.; Larabi, C.; Quadrelli, E. A.; Bonino, F.; Lillerud, K. P. Synthesis and Stability of Tagged UiO-66 Zr-MOFs. *Chem. Mater.* **2010**, *22*, 6632−6640.
(44) Kim, M.; Cahill, J. F.; Fei, H.; Prather, K. A.; Cohen, S. M. Postsynthetic Ligand and Cation Exchange in Robust Metal-Organic Frameworks. *J. Am. Chem. Soc.* **2012**, *134*, 18082−18088.
(45) DeStefano, M. R.; Islamoglu, T.; Hupp, J. T.; Farha, O. K. Room-Temperature Synthesis of UiO-66 and Thermal Modulation of Densities of Defect Sites. *Chem. Mater.* **2017**, *29*, 1357−1361.
(46) Taddei, M.; Wakeham, R. J.; Koutsianos, A.; Andreoli, E.; Barron, A. R. Post-Synthetic Ligand Exchange in Zirconium-Based Metal-Organic Frameworks: Beware of the Defects! *Angew. Chem., Int. Ed.* **2018**, *57*, 11706−11710.
(47) Wu, H.; Chua, Y. S.; Krungleviciute, V.; Tyagi, M.; Chen, P.; Yildirim, T.; Zhou, W. Unusual and Highly Tunable Missing-Linker Defects in Zirconium Metal-Organic Framework UiO-66 and Their Important Effects on Gas Adsorption. *J. Am. Chem. Soc.* **2013**, *135*, 10525−10532.
(48) Shearer, G. C.; Chavan, S.; Ethiraj, J.; Vitillo, J. G.; Svelle, S.; Olsbye, U.; Lamberti, C.; Bordiga, S.; Lillerud, K. P. Tuned to Perfection: Ironing out the Defects in Metal-Organic Framework UiO-66. *Chem. Mater.* **2014**, *26*, 4068−4071.
(49) Shearer, G. C.; Chavan, S.; Bordiga, S.; Svelle, S.; Olsbye, U.; Lillerud, K. P. Defect Engineering: Tuning the Porosity and Composition of the Metal-Organic Framework UiO-66 via Modulated Synthesis. *Chem. Mater.* **2016**, *28*, 3749−3761.
(50) Perfecto-Irigaray, M.; Beobide, G.; Castillo, O.; da Silva, I.; Garcia-Lojo, D.; Luque, A.; Mendia, A.; Perez-Yanez, S. $[Zr_6O_4(OH)_4(Benzene\text{-}1,4\text{-}Dicarboxylato)_6]_N$: A Hexagonal Polymorph of UiO-66. *Chem. Commun.* **2019**, *55*, 5954−5957.
(51) Katz, M. J.; Brown, Z. J.; Colon, Y. J.; Siu, P. W.; Scheidt, K. A.; Snurr, R. Q.; Hupp, J. T.; Farha, O. K. A Facile Synthesis of UiO-66, UiO-67 and Their Derivatives. *Chem. Commun.* **2013**, *49*, 9449−9451.
(52) Schaate, A.; Roy, P.; Godt, A.; Lippke, J.; Waltz, F.; Wiebcke, M.; Behrens, P. Modulated Synthesis of Zr-Based Metal-Organic Frameworks: From Nano to Single Crystals. *Chem. - Eur. J.* **2011**, *17*, 6643−6651.

https://dx.doi.org/10.1021/acsmaterialslett.0c00012
ACS Materials Lett. 2020, 2, 499−504